Article

Equilibrium and Kinetics of DNA Overstretching Modeled with a Quartic Energy Landscape

David Argudo[1] and Prashant K. Purohit[1,*]
[1]Department of Mechanical Engineering and Applied Mechanics, University of Pennsylvania, Philadelphia, Pennsylvania

ABSTRACT It is well known that the dsDNA molecule undergoes a phase transition from B-DNA into an overstretched state at high forces. For some time, the structure of the overstretched state remained unknown and highly debated, but recent advances in experimental techniques have presented evidence of more than one possible phase (or even a mixed phase) depending on ionic conditions, temperature, and basepair sequence. Here, we present a theoretical model to study the overstretching transition with the possibility that the overstretched state is a mixture of two phases: a structure with portions of inner strand separation (melted or M-DNA), and an extended phase that retains the basepair structure (S-DNA). We model the double-stranded DNA as a chain composed of n segments of length l, where the transition is studied by means of a Landau quartic potential with statistical fluctuations. The length l is a measure of cooperativity of the transition and is key to characterizing the overstretched phase. By analyzing the different values of l corresponding to a wide spectrum of experiments, we find that for a range of temperatures and ionic conditions, the overstretched form is likely to be a mix of M-DNA and S-DNA. For a transition close to a pure S-DNA state, where the change in extension is close to 1.7 times the original B-DNA length, we find $l \approx 25$ basepairs regardless of temperature and ionic concentration. Our model is fully analytical, yet it accurately reproduces the force-extension curves, as well as the transient kinetic behavior, seen in DNA overstretching experiments.

INTRODUCTION

Under physiological conditions inside the cell, the prevalent double-stranded (ds)DNA conformation is the B-DNA form, a right-handed double helix with ~10.5 basepairs (bp) per helical turn and ~0.34 nm per basepair. When B-DNA is subjected to external stress conditions it can undergo conformational changes into other DNA forms (1). A key experiment used for the study of DNA response is one in which a tensile force is applied on the DNA, leading to an elastic regime of increasing extension and eventually to what has been denominated in the literature as an overstretching transition from B-DNA to an elongated form (2).

The force-extension curve of DNA has been extensively studied in the literature by both experimental and theoretical methods, and we refer the reader to Bustamante et al. (2) for a more detailed review regarding the advances in the study of DNA under tension. Some of the pioneering experimental work regarding the overstretching transition was performed by Smith et al. (3), Williams et al. (4,5), and Rouzina and Bloomfield (6). Parallel to the experimental discovery of the overstretching transition, Cluzel et al. (7) presented a theoretical model analogous to the helix-coil transition model. Since then, the majority of the theoretical efforts discussing the DNA overstretching transition are based on models such as the Zimm-Bragg theory or Ising models, where the theory is adapted to include entropic elasticity effects. Ahsan et al. (8) and Marko (9) included entropic elasticity by means of the wormlike chain (WLC), where both states were assumed to have the same flexural rigidity of B-DNA. Rouzina and Bloomfield (6) combined the Zimm-Bragg model with both the WLC model and the freely joined chain to describe overstretching, whereas Storm and Nelson (10,11) and Cizeau and Viovy (12) presented an Ising-type model where each state can have arbitrary elastic constants. In addition to helix-coil type models, simulations of a dynamical Langevin model using a Landau-Ginzburg landscape (13) and simulations of a dynamical model using a Peyrard-Bishop-Dauxois mesoscopic model for the energy potential (14) have also been proposed to describe the DNA transition at high forces.

The coarse-grained simulations of Whitelam et al. (15–17) have provided important insights into the competition between different overstretching modes. These authors present a model of DNA with basepair resolution in which kinetics of the overstretching transition are explored using a Monte Carlo scheme. Their methods allow us to discriminate between the dynamics associated with the DNA overstretching transition to hybridized and unhybridized structures (15–17), while including the effects of basepair sequence and heterogeneity. Finally, with the objective of providing a deeper structural explanation at the microscopic level, DNA overstretching phenomena have also been studied using atomistic modeling (18), by means of molecular-modeling treatments with implicit solvent representations (19–21) and by using molecular-dynamic simulations

Submitted May 23, 2014, and accepted for publication September 16, 2014.
*Correspondence: purohit@seas.upenn.edu
Editor: Sean Sun.

0006-3495/14/11/2151/13 $2.00
http://dx.doi.org/10.1016/j.bpj.2014.09.014

(21–23). The initial steered molecular-dynamic simulations used to study the DNA overstretching phenomena (22–24) gave transition forces one order-of-magnitude larger than the experimental ones. Simulations in which the free-energy profile of the system was determined using an umbrella sampling technique have recently provided a more realistic picture of the overstretching transition (24).

With advances in experimental techniques, the interest in the overstretching transition has peaked in recent years, and it has been argued that B-DNA can undergo more than one overstretching transition. Zhang et al. (25,26), Fu et al. (27), and King et al. (28) have been using single-molecule methods to study the overstretching transition, reaching the conclusion that DNA can undergo three types of transitions:

B-DNA to peeled DNA (single-stranded DNA or ssDNA);
B-DNA to melted DNA (M-DNA, inside strand separation in the form of bubbles); and
B-DNA to S-DNA (nonhysteretic transition).

The experiments can be done in such a fashion that peeling is not topologically allowed in what the authors call an "end-closed setup" (26). It was established that even in the case of end-opened DNA (which does not preclude peeling topologically), unpeeling is suppressed with increasing ionic strength (28). It has also been shown that when the content of (AT) tracts is high, a force-induced melting transition is prevalent, whereas sequences with a higher GC content undergo a nonhysteretic overstretch transition into the S-form (28,29).

Similar results regarding the preferred overstretched state depending on temperature, DNA sequence, and ionic concentration were reached in the coarse-grained simulations by Whitelam et al. (15–17). The different overstretching transitions seem to be characterized by different levels of cooperativity and kinetic behavior (30). Bianco et al. (31) and Bongini et al. (32) studied the transition kinetics of the overstretching transition using force-steps in pulling experiments of λ-DNA (~48.5 kbp), where they found that the cooperative length of the B-to-S transition is ~22–25 bp. The experimental findings of Bianco et al. (31) and Bongini et al. (32) have been recently satisfactorily reproduced using atomistic molecular-dynamics simulations (24).

Cooperativity during a phase transition is defined as the phenomenon in which some property changes gradually (in a sigmoidal way) as a function of the external controlled parameter (33). This means that certain regions of the system are somehow tied together in such a way that the driving force on a region to undergo the phase transition is directly influenced by whether other regions have undergone the conformational changes (34). A system in which n identical subunits undergo a phase transition in perfect unison is denominated as perfectly (maximum) cooperative. If the transition is less cooperative, the gradual change of the parameter during the transition would be less steep. Therefore, during a phase transition one can define a cooperative unit for the transition (34). This unit of cooperativity reflects the size of the subunits that undergo the conformation changes completely independently of one another. In the case of a DNA filament undergoing a two-state phase transition, the cooperative unit size is the number of basepairs that will transition as a single unit.

In this article, we focus on the regime where peeling is not allowed, and we present a theoretical model applicable to the B-to-S and B-to-M transitions, where we assume that at high forces the bending effects can be neglected. In our cooperative system the property that varies in a sigmoidal fashion is the extension of the DNA molecule as a function of the applied force, where the cooperative unit size is defined by the length l (in number of basepairs) of independent segments n that make up the total DNA chain. For a highly cooperative overstretching transition the value of l is expected to be large, leading to a small number of interfaces, meaning there is a high energetic cost of creating an interface between two states (34). The main objective of our work is to obtain the value of the cooperative unit l. To achieve this, we developed an analytical continuous two-state model for the DNA overstretching transition, in which we account for the global statistical fluctuations of the system due to thermal effects.

We compare our model to overstretching experiments to obtain the values of l. Our results are in excellent agreement with independent experimental measures of the cooperative unit l for dsDNA overstretching transitions (30–32). Furthermore, in agreement with recent experimental evidence (26,28,32), our predictions of l support the notion that the overstretched state is a mixed DNA form at the temperature range and ionic concentrations used in various experiments. We find that l varies depending on whether the B-DNA undergoes a transition closer to a pure S form, or a transition closer to the M form. Hence, we argue that the cooperativity value l is not only a measure of the energetic cost of creating an interface (34) between B-DNA and the overstretched state, but it is also a key physical parameter that characterizes the fraction of the phases in the overstretched state. Finally, we connect our model with Kramer's rate theory for stochastic systems with double-well potentials (35) to describe the kinetics of the system. We find that the resulting analytical model using our predicted l values accurately reproduces the kinetic behavior seen in experiments of Bianco et al. (31) and Bongini et al. (32).

MODEL DESCRIPTION

The DNA in the overstretching experiments is modeled as a continuous and extensible rod, where s is the arc length along the centerline of the rod in the reference B-DNA configuration. This rod (dsDNA filament) is subject to

thermal fluctuations and high tensions depicted in the inset of Fig. 1. Our problem is to evaluate the partition function and free energy of such a rod assuming that the energy can be expressed as a quartic function of the order parameter $u(s)$. The variable u is a nondimensional measure of the stretch of the rod (see Experimental Observables: DNA Extension Z), which not only characterizes the rod configuration, but is also the reaction coordinate describing the onset of a phase transition driven by the applied tension F.

Energy of the system

In this model, the DNA is assumed to be torsionally unconstrained such that there is no twist in the molecule. In the undeformed initial configuration, the DNA is in the B state in which its length is given by $L = N \times$ bp, with N being the number of basepairs and bp $\approx$ 0.34 nm, the length of each basepair. We constrained our model for a regime of moderate to high forces $F >$ ~15 pN. In this regime, the shortening of DNA due to thermal bending fluctuations is negligible. Next, we proceed with a mean-field Hamiltonian for the energetics of the system:

$$\begin{aligned} H &= [V(u) + Cu]L, \\ V(u) &= A_4u^4 - A_2u^2. \end{aligned} \tag{1}$$

Here $u(s)$ plays the role of the order parameter and it is a measure of the filament's stretch (see Eq. 5) and $V(u)$ represents the strain energy density. In writing Eq. 1, we have assumed that the filament's deformation is homogeneous such that u and $V(u)$ are independent of the arc-length s.

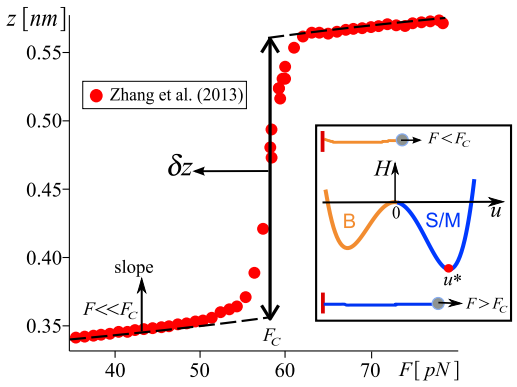

FIGURE 1 Procedure to fit values of A_2 and A_4. (*Data points*) Experiments by Zhang et al. (26) at $I = 3.5$ mM and $T = 12°C$, where the critical force $F_c \approx 57.5$ pN. (*Dashed lines*) Extension z assuming no thermal fluctuation (see Eq. 5). We fit $A_2 = 93$ pN and $A_4 = 500$ pN to the slope (far from the transition point) and to the change in extension δz between the compact and extended states. (*Inset*) Schematic of double-well potential modeling the overstretching experiment. For $F < F_c$, the system is in the B-DNA state. As the force increases, for $F > F_c$, the right well of the potential H is deeper as shown in the figure and the molecule transitions into the overstretched state. The right well represents the global minimum u^* in the overstretched form (S/M stands for S-DNA or M-DNA) and the left well corresponds to the local equilibrium of u in the B-form. To see this figure in color, go online.

A discrete version of the Hamiltonian given in Eq. 1 has been used in DNA overstretching dynamic simulations (13). A_4, A_2, and C are phenomenological parameters to be evaluated by comparing to the overstretching experiments. The value of A_4 must be positive to satisfy the conditions of stability.

Homogeneous equilibrium solutions

The homogeneous equilibrium stretch value u^* simply corresponds to the value of u that minimizes the potential $H(u)$, where C plays the role of the external field:

$$\left.\frac{dH}{du}\right|_{u=u^*} = 4A_4(u^*)^3 - 2A_2(u^*) + C = 0. \tag{2}$$

For $C = 0$, Eq. 2 has one unstable solution, $u_b = 0$, and two stable minima, $\pm u_o$:

$$u^*|_{C=0} = \pm u_o = \pm\sqrt{\frac{A_2}{2A_4}}. \tag{3}$$

DNA overstretching transitions: changes in temperature and salt concentration

Within the Landau framework of phase transitions, any of the parameters A_4, A_2, or C, appearing in the phenomenological potential $V(u)$, can be a function of the controlled external variables (36). In the DNA stretching experiments that we will consider, the controllable external variables are the force F, ionic solution concentration I, and temperature T. Inasmuch as u is related to the extension of the filament (see Eq. 5), it is clear that the external field F must contribute through the linear term in the Hamiltonian, such that $C = -F +$ other terms. Furthermore, the effects of temperature T and salt concentration I will come through the linear term as well. This is analogous to what is seen in the Landau model of liquid-vapor systems (37). Therefore, we assume a general form for $C(F, T, I)$:

$$C = f(T, I) - F. \tag{4}$$

The exact form of $f(T, I)$ is taken from the phenomenological relationships found in experiments (25,26,31,32). In the experiments, one of the variables T or I is constant whereas the other one can be varied. At the onset of the transition, the energy wells of the B-DNA state and overstretched DNA state have equal depth and the system has two global minima given by Eq. 3. Therefore, the transition midpoint is given by the condition that $C = 0$ or equivalently $F_c = f(i)$, where $I = \{I, T\}$, depending on whether the controlled variable is the temperature T or the salt concentration I. The value of the critical force F_c at which the transition takes place depends strongly on I and T (25,26,32). Instead of using a general phenomenological equation for all experimental data, we have used the value $f(i) = F_c$ as measured

in each experiment. We do so because different groups reported different phenomenological behavior for similar experimental conditions (25,32). A brief description of the empirical relations among the critical force F_c, temperature T, and concentration I is given in Section S2, Empirical Expressions for the Critical Force as a Function of Temperature and Ionic Concentration in the Supporting Material.

Experimental observables: DNA extension *z*

There are two types of stretching experiments: extension-controlled and force-controlled. We will focus mainly on recent experiments where F is controlled and the end-to-end extension z is measured (25,26,32). The relationship between the order parameter u and the extension of the molecule z is given by

$$z = (1 + u^* - u^*\big|_{F=\widehat{F}})\text{bp}, \tag{5}$$

where bp $\approx$ 0.34 nm is the basepair length in the B-DNA state and $u^*(F)$ is the global minimum in Eq. 2. The order parameter u is a measure of stretch with reference to a midpoint between compact (B) and extended states (S or M) as shown in the inset to Fig. 1. To set the reference state with zero stretch to be the B-form, where $z = \text{bp[nm]}$, u^* must be shifted by a constant. Therefore, the shifting constant $u^*\big|_{F=\widehat{F}}$ (u^* evaluated at $F = \widehat{F}$) ensures the condition of zero stretch in the system at the initial B-DNA configuration ($L = N \times$ bp). The value of the force at which $z \approx 0.34$ nm as seen in DNA extension experiments is $\widehat{F} \sim 15$ pN. Note that $\widehat{F} >> 1$ pN, inasmuch as thermal fluctuations would effectively shorten the DNA length in the small force regime. To distinguish between the B and overstretched forms, the length of the overstretched form after the transition is complete is labeled $\overline{L}$.

Next we describe the procedure to fit the values of the parameters A_2 and A_4 to the experimental overstretching curves $z(F)$. The first equation is provided by the difference in value of z (between the two states) at the midpoint of the transition ($C = 0$). The change in extension δz between the compact and extended form is approximately

$$\delta z \approx \left(\overline{L} - L\right)/N = \left|2u_o\right|\text{bp}, \tag{6}$$

where u_o is the equilibrium solution of the order parameter given by Eq. 3 and it is a function of A_2 and A_4. The second equation is provided by an analysis of the low-force regime ($F << F_c$), where the filament is in the B-form. Far away from the transition point, the slope of $z(F)$ is not affected by the statistical fluctuations of u and it can be obtained from the parameters A_2 and A_4 using the zero-temperature model. Analogously to the stretch modulus in the WLC theory (3,38), at high forces ($F > 15$ pN) where bending effects are small, A_2 and A_4 quantify the change in extension $z(F)$. We found that $A_4 \approx 500$ pN consistently provided a good fit for the force-extension slope for all the experimental curves used in this study. Therefore, in the following sections we will use $A_4 \sim 500$ pN, and let A_2 be the parameter that dictates the change in extension δz between the B-state and the overstretched state. To illustrate this procedure, in Fig. 1 we fit the values of A_2 and A_4 to one of the experimental data sets from Zhang et al. (26).

So far we have described the zero-temperature model, which neglects thermal fluctuations. In Methods: Statistical Mechanics of the Chain we include the contributions of the global statistical fluctuations of the order parameter u due to thermal effects and describe an analytical procedure to compute the average extension $\langle z \rangle$ as a function of the controlled parameters and the cooperative unit l.

METHODS: STATISTICAL MECHANICS OF THE CHAIN

We model our DNA filament as a chain made of n segments of length l, where each segment is identical to others and each segment can be easily identified and labeled along the arc-length s. The Hamiltonian of a single segment j is given as

$$H_j = \left[A_4 u_j^4 - A_2 u_j^2 + C(F,T,I)u_j\right]l, \tag{7}$$

where we assume that each segment j undergoes a homogeneous deformation such that u_j is independent of s. Then the total energy E of the n noninteracting distinguishable segments is

$$E = \sum_{j=1}^{n} H_j.$$

We assume that each segment is an independent subsystem with its own specific set of boundary conditions that does not interact with other subsystems. We focus on a single subsystem where the phase change occurs by the passage of a single phase boundary (maximum cooperativity within each subsystem). Therefore, the length l is a measure of the cooperativity in our model. If we further assume that the subsystems are identical, then the partition function of the chain of identical but distinguishable noninteracting segments is given by $Z_s = Z^n$ (39), where Z is the partition function of a single segment j described in detail in the next section.

Partition function *Z* of a segment of length *l*

The order parameter in Eq. 7 is a continuous variable, therefore taking the sum over all possible configurations of $u_j(s)$

in the continuous limit yields the partition function of a single segment to be

$$Z = \int_{-\infty}^{+\infty} \exp\left[-\beta l\left(A_4u^4 - A_2u^2 + Cu\right)\right]du, \quad \beta = \frac{1}{k_BT}, \tag{8}$$

where k_B is the Boltzmann constant and, for convenience, we have dropped the j index. Next, to evaluate Eq. 8, we follow the methods in Tuszynski et al. (37) and define the variables:

$$a = A_4\beta l, \ b = -A_2\beta l, \ \text{and} \ c = C\beta l. \tag{9}$$

Then the partition function of the system can be rewritten by performing a Taylor expansion on the linear term of the Hamiltonian:

$$Z = \sum_{n=0}^{\infty}\frac{(-c)^n}{n!}\int_{-\infty}^{+\infty} u^n\exp\left[-au^4 - bu^2\right]du. \tag{10}$$

It is clear from Eq. 10 that when n is odd, $Z = 0$. When $n = 2m$ is even, the solution to each one of the integrals in the summation of Eq. 10 can be found in Ryzhik and Gradshteyn (40), such that $Z|_{n=2m} = Z_m$,

$$Z_m = \sum_{m=0}^{\infty}\frac{(-c)^{2m}}{(2m)!}\frac{\Gamma(m+1/2)}{(2a)^{(2m+1)/4}}\exp\left(\frac{q^2}{4}\right)U(m,q), \tag{11}$$

where $U(m,q) = D_{-m=1/2}(q)$ is the parabolic cylinder function (41). We can simplify this expression further by making use of the properties of the $\Gamma(x)$ function

$$\Gamma\left(m+\frac{1}{2}\right) = \frac{\sqrt{\pi}}{4^m}\frac{(2m)!}{m!}, \tag{12}$$

such that the partition function of an individual segment of length l is

$$Z_m = \left[\frac{\pi^2}{2A_4\beta l}\right]^{1/4}\sum_{m=0}^{\infty}\left[\frac{Q^m}{m!}\exp\left(\frac{q^2}{4}\right)U(m,q)\right], \tag{13}$$

where

$$Q = (\beta l)^{3/2}\frac{[C(F,T)]^2}{4\sqrt{2A_4}} \ \text{and} \ q = A_2\sqrt{\frac{\beta l}{2A_4}}. \tag{14}$$

(Equation 13 is an exact result, but near the transition midpoint ($C \sim 0$) evaluating the sum up to $m = 2$ suffices to capture the transition behavior.)

Finally, the ensemble free energy of each subsystem is

$$G = -\beta^{-1}\ln Z_m. \tag{15}$$

Force-extension relation for the chain undergoing the overstretching transition

Once the free energy G is known, one can compute the average value of conjugate variable $\langle u\rangle$ to the external field C:

$$\langle u\rangle = -\frac{1}{l}\frac{\partial G}{\partial C}. \tag{16}$$

The procedure to obtain $\langle u\rangle$ follows from using Eqs. 13 and 15,

$$\beta G = \frac{1}{2}\ln\pi - \frac{1}{4}\ln(2a) + \ln\Psi, \tag{17}$$

where

$$\Psi = \sum_{m=0}^{\infty}\left[\frac{Q^m}{m!}\exp\left(\frac{q^2}{4}\right)U(m,q)\right]. \tag{18}$$

Next, by means of the chain rule,

$$\begin{aligned}\beta\frac{\partial G}{\partial C} &= \Psi^{-1}\frac{\partial\Psi}{\partial c}\frac{\partial c}{\partial C}\\ &= \frac{cl\beta}{\Psi\sqrt{8a}}\sum_{m=1}^{\infty}\left[\frac{Q^{m-1}}{(m-1)!}\exp\left(\frac{q^2}{4}\right)U(m,q)\right].\end{aligned} \tag{19}$$

We can simplify these expressions further by making use of the definition $\Gamma(x) = (x-1)!$ and the relations in Eq. 9, such that the average value of the order parameter is

$$\langle u\rangle = \left[\frac{(l\beta)^{1/2}C}{\Psi\sqrt{8A_4}}\right]\sum_{m=1}^{\infty}\left[\frac{Q^{m-1}}{\Gamma(m)}\exp\left(\frac{q^2}{4}\right)U(m,q)\right], \tag{20}$$

where Ψ is given by Eq. 18 and Q,q values are defined in Eq. 14. Finally, replacing u^* with the expected value $\langle u\rangle$ in Eq. 5, we can compute the average end-to-end extension:

$$\langle z\rangle = (1 + \langle u\rangle - u^*|_{F=\widehat{F}})bp. \tag{21}$$

In Results and Discussion, we compare our model to the experiments with C as defined by the phenomenological expression in Eq. 4.

RESULTS AND DISCUSSION

Our strategy to obtain the cooperative unit l from the experimental data is the following. First, we fit A_2 and A_4 using a zero-temperature model as described in Experimental Observables: DNA Extension Z. Next, for convenience, we shift the extension experimental curves by the value of the critical force F_c corresponding to each experiment. Then the extension $\langle z\rangle$ can be expressed as a function of $\Delta F = F - F_c$. Finally, combining Eqs. 20 and 21, we fit l (the only unknown in the system) to the experimental curves. In Fig. 2 *a*, we show the fitting of our statistical model to

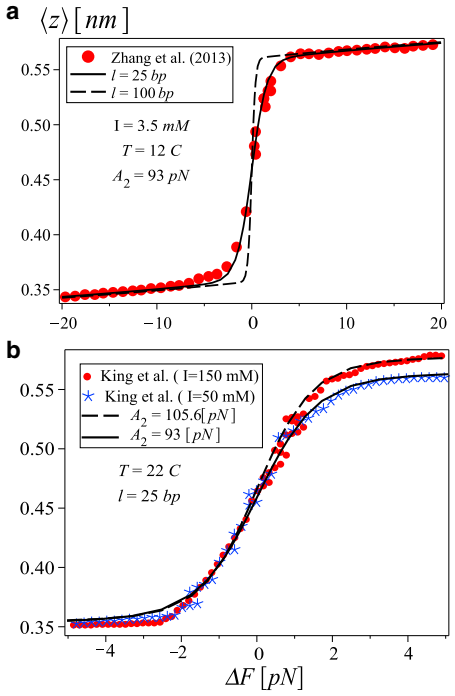

FIGURE 2 Force-extension relation during dsDNA overstretching. (*a*) Theoretical predictions for experiments from Zhang et al. (26) for l = 25 bp (*solid*) and l = 100 bp (*dashed*); same conditions as in Fig. 1. (*b*) Two experiments in King et al. (28) (*data points*); theoretical predictions from our model (*lines*) using l = 25 bp. Here F_c = 69.5 pN at 50 mM and F_c = 63.5 pN at 150 mM. To see this figure in color, go online.

the same experimental curve presented earlier in Fig. 1. The force-extension prediction with $l \approx 25$ bp agrees very well with the data-set in Zhang et al. (26). Through different methods and at different ionic conditions I = 150 mM, Bianco et al. (31) and Bongini et al. (32) measured the cooperativity length to be $l \in [22, 25]$bp. They found that this value of l is essentially independent of temperature for $T \in [22, 25]$°C. Another group, Rouzina et al. (30), reported that the B-to-S transition is characterized by a slightly lower value of $l \approx 10$ bp and that the B-to-M transition is much more cooperative where $l \approx 100$ bp. Because $l = 25$ bp is between the two reported values for B-to-S and B-to-M in Rouzina et al. (30), we consider the possibility that the overstretched state, in the experimental data in Fig. 2 *a* and the experiments in Bianco et al. (31) and Bongini et al. (32), is a mixture of S and M. In fact, recent experimental findings strongly support the idea of a mixed overstretched form. In the next section we briefly review some of the experimental results behind this idea.

DNA overstretching transitions: B-to-S, B-to-M, or both

Although there is conclusive evidence that S-DNA exists and that it is favored at high salt concentration and low temperatures, and that M-DNA can also be present in force-induced transitions for lower salt concentrations and high temperatures (25,26,28,29), there are still some unanswered questions regarding the structure of the overstretched state. In Table 1, we list some of the experiments that present the possibility of a mixed S and M state after the overstretching transition. For instance, M-DNA was present in a nonhysteretic transition (28), whereas in Zhang et al. (26) hysteresis was always seen in a significantly shorter M-DNA. As pointed out in Zhang et al. (26), the difference could be explained if there was a mixture of S and M in the overstretching experiment in King et al. (28). Furthermore, in Bianco et al. (31) and Bongini et al. (32), the overstretched length was ~1.7 times the B-DNA form for both hysteretic and nonhysteretic transitions and the authors' kinetic data suggest two processes during the overstretching transition. The idea of S and M state coexistence is further supported by the gradual change in extension of the overstretching curves in Zhang et al. (26) as a function of ionic concentration. Based on these experimental facts we think our model will be useful in using the cooperative length l to quantify the mixing of S and M DNA after the transition.

Cooperativity length *l* predictions

Next, we present some ideas that emerged when we used our model to analyze the DNA overstretching curves of various groups.

Regardless of temperature T, length L, or ionic concentration I, for experimental curves where the change in extension is $\overline{L} \approx 1.7\,L$ the cooperativity of the system is given approximately by $l \in [22–25]$bp. Although T, I, and L are different among the data sets presented in Fig. 2, the three sets are quantitatively reproduced by our model using

TABLE 1 Summary of recent DNA overstretching experiments used throughout this study

Reference (figure)	T [°C]	I [mM]	L [kbp]	Description	$\overline{L}$
Zhang et al. (see Fig. 3b (26))	24	150	~7.3	Nonhysteretic (S-DNA)	~1.7
Zhang et al. (see Fig. 3b (26))	24	1.0	~7.3	Hysteretic (M-DNA)	~1.5
Zhang et al. (see Fig. 3c (26))	12	3.5	~7.3	Nonhysteretic (S-DNA)	~1.7
King et al. (see Fig. 1a (28))	22	50	~48.5	Nonhysteretic (M-DNA)	~1.7
King et al. (see Fig. S4 (28))	22	150	~25	Nonhysteretic (S-DNA)	~1.7
Bongini et al. (32)	10–25	150	~48.5	Nonhysteretic and hysteretic	~1.7
Zhang et al. (25)	10–20	500	~48.5	Nonhysteretic (S-DNA)	~1.7

L is the length in the B-DNA state and $\overline{L}$ is the length of the DNA filament after the transition measured in L units.

$l \approx 25$ bp. Similarly, Fig. 3 *a* shows that using $l \approx 22$ bp accurately reproduces experiments from Zhang et al. (26) at $I = 150$ mM and $T = 22°C$. Furthermore, using $l \approx 22$ bp in Fig. S1 in the Supporting Material, we show that experiments from Bianco et al. (31) and Bongini et al. (32) at $I = 150$ mM and $T = 22°C$ are consistent with experiments in Zhang et al. (26) and King et al. (28).

The experimental data in Zhang et al. (26) showed a gradual change in $\langle z \rangle$ as a function of ionic concentration. This is shown in Fig. 3 where we fit data from Fig. 3 *b* in Zhang et al. (26). In Zhang et al. (26), at the low ionic concentrations, there is an asymmetric pattern in the force-extension curves when the force increases and then decreases. This hysteretic behavior observed during overstretching is due to the slow convergence to equilibrium (13,42). The asymmetric hysteresis at $I = 1$ mM and $I = 5$ mM in Zhang et al. (26), where the system is out of equilibrium mainly during unloading, is consistent with previous stretching experiments that depict marked hysteresis during the decreasing force regime (5,14,31,32,43,44).

During the loading phase in some of these experiments, there are no hysteretic effects, whereas in others, if hysteresis is present, its effect is significantly less pronounced than during unloading. Therefore, for the low $I = 1$ and 5 mM we fit only to the pulling data in Zhang et al. (26). As shown in Fig. 3, l decreases gradually with increasing I, ranging from $l \approx 60$ bp at $I = 1$ mM down to $l \approx 22$ bp at $I = 150$ mM. The smaller cooperativity values are consistent with $\overline{L} > 1.7\,L$. Given that experiments (26,28,30) confirm that the S-form is preferred at high salt concentrations and that the S form is mainly responsible for the 1.7 times change in extension (32), we conclude based on our fittings that

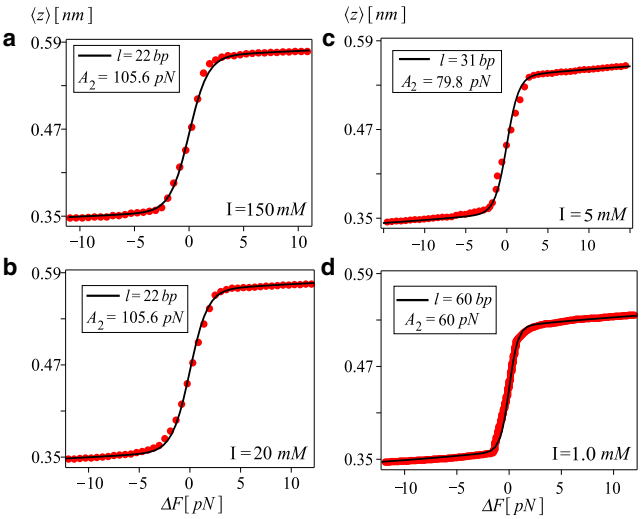

FIGURE 3 DNA overstretching at $T = 24°C$ for different ionic concentrations. (*Red markers*) Experiments from Zhang et al. (26); (*solid lines*) theoretical predictions from our model. As the ionic strength decreases going from panels *a–d*, A_2 decreases and l increases. We use $A_4 \sim 500$ pN and F_c as measured in experiments: $F_c = [68.3, 63.5, 58.8, 50.5]$ pN going from panels *a–d*. To see this figure in color, go online.

for $l < 30$ bp the predominant state in the overstretched form is S-DNA.

As the transition becomes less cooperative, the increase in l of each subsystem has the same theoretical effect as drastically decreasing the temperature T, as evidenced from the definition of the partition function given in Eq. 8. A change of four times in the value of l from 25 to 100 bp is equivalent to a decrease of the absolute temperature from room temperature to $T = 75$ K, which effectively yields less global statistical fluctuations. Thus, one can expect the sigmoidal curve to sharpen and become closer to an abrupt first-order phase transition. In Fig. 2 *a* we have plotted the curve for $l = 100$ bp next to the 25-bp solution, so that the difference in width of the curves is apparent.

Although moderate changes in temperature $T \in [10–25]°C$ affect the critical force F_c value (26,32), the change of temperature in this range does not seem to affect the extension of the molecule up to $T = T_M$ at fixed I (see Fig. 3c in Zhang et al. (26)). But once $T \geq T_M$, there is a sudden change in the extension profile of the overstretching curves (26). The data of Bongini et al. (32) and Zhang et al. (25) support the idea that, at a fixed I for a range of temperatures $T \in \sim[10–25]°C$, the extension of the overstretched form remains approximately the same. This would imply that given a fixed I, there is a single transition class to the S-form (or at least closer to pure S) for $T < T_M$ and a melting transition for $T > T_M$. Hence, we think of l as independent of T for each transition class, and making use of the phenomenological model for $C(F, T)$ as described in DNA Overstretching Transitions: Changes in Temperature and Salt Concentration, we predict the behavior of the overstretching transition as a function of T. A sample of the results is shown in Fig. S3, where we show that introducing the temperature effects through $C(F, T)$ captures what is seen in experiment.

At higher ionic concentrations ($I = 500$ mM (25)), we found that although $l = 22$ bp is a good average fit to the experimental data, the curve is not symmetric about the midpoint of the transition and the data is better fit by $l \approx 15$ bp near the overstretched state (Fig. 4). Similar behavior is found in the overstretching curve from King et al. (28) at $T = 22°C$ and $I = 1$ M. However, this asymmetric aspect of the overstretching transition is much more evident in Fig. 5, where we present the comparison of the variance measurements of Zhang et al. (25) with our theoretical predictions. Because the n segments making up the entire chain are independent of one another, the system is analogous to a random walk of n steps. In this analogy, the average step size of the walker is $\langle ul \rangle$ and the variance of each step equals the variance of one segment of length l,

$$\sigma_l^2 = l^2\left(\langle u^2 \rangle - \langle u \rangle^2\right), \tag{22}$$

where $\langle u^2 \rangle = d(\ln Z_m)/db$ is the second moment of the partition function and b is defined in Eq. 9. Then the variance for the entire chain (n-steps) is (45)

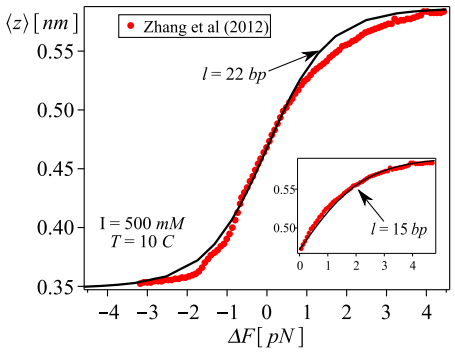

FIGURE 4 Force-extension curve fit to the experiments from Zhang et al. (25) at higher salt concentration. We have used $A_2 = 120$ pN and $F_c = 67.2$ pN. Although $l \approx 22$ bp provides a good overall fit, using $l \approx 15$ bp provides better agreement in the upper-right section of the curve (shown in the *inset*). To see this figure in color, go online.

$$\sigma_\nu^2 = n\sigma_l^2 = L\left(\langle u^2\rangle - \langle u\rangle^2\right)l. \tag{23}$$

For a given force, because L is fixed, the variance grows linearly with the cooperativity length. In Fig. 5, gray circles correspond to the experimental measurements from Zhang et al. (25) of the variance at $I = 500$ mM. Lines correspond to our theoretical predictions for different values of l using Eq. 23. The red solid line (for $l = 15$ bp) agrees strongly with the experimental data for $\Delta F > 0$ (*right side* of the graph), whereas on the left side of the graph the blue solid line (for $l = 30$ bp) provides a better fit. The black solid line ($l = 22$ bp) in Fig. 5 is shown as an average fit for both sides of the graph.

An alternative method to quantify the cooperativity of the DNA overstretching transition is to use the Zimm-Bragg parameter σ_F (6),

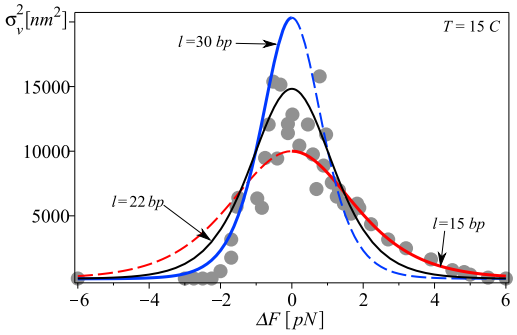

FIGURE 5 Variance σ^2_ν as a function of the force. (*Points*) Experimental measurements at $I = 500$ mM of Zhang et al. (25). (*Lines*) Theoretical predictions for different values of l using Eq. 23. (*Red solid line*) $l = 15$ bp agrees strongly with the experimental data for $\Delta F > 0$ (*right side* of the graph; *left side* of the graph, *blue solid line*); $l = 30$ bp provides a better fit. The asymmetric fitting to the variance is in agreement with the results shown for the force extension curves at the same high ionic conditions in Fig. 4. (*Black solid line*) $l = 22$ bp is shown as an average fit for both sides of the graph. To see this figure in color, go online.

$$\sigma_F = \exp(-2\beta E_s), \tag{24}$$

where $2E_s$ is the energetic cost involving two junctions (this is the definition given in Khokhlov and Grosberg (46)). In qualitative terms, large values of a cooperative unit l are analogous to small values of σ_F (34), but a quantitative relation can be obtained by the following procedure. The parameter σ_F reflects the width δF of the overstretching transition in terms of the force (6,46). The value δF can be determined by the midpoint slope of the plot P_s versus F (6,46), where P_s is the fraction of the filament in the overstretched state. Then the force transition width is (6)

$$\delta F = \frac{\partial F}{\partial P_s}\Big|_{F=F_c} = 4\sigma_F^{1/2}\frac{k_B T}{\delta z}, \tag{25}$$

where δz is the change in extension per basepair during the transition. Instead of using δz as approximated before in the zero-temperature calculations, the model presented in Methods: Statistical Mechanics of the Chain allows us to provide a closer-to-exact estimate for δz,

$$\delta z = \langle u_f\rangle - \langle u_i\rangle, \tag{26}$$

where the subscripts i and f stand for initial and final point of the transition, respectively. Using the definition of P_s given by Odijk (38), we can directly compute δF by the left equality in Eq. 25. Next, making use of Eq. 20, we can evaluate $\langle u_i\rangle$ and $\langle u_f\rangle$ at $F_i = F_c - \delta F/2$ and $F_f = F_c + \delta F/2$, respectively. By doing so, Eq. 25 directly links our methods to the Zimm-Bragg cooperativity model, and we can calculate the parameter σ_F as a function of l. In Table 2, we present δF and σ_F for several sets of experimental data used throughout this article, where we see that σ_F is $\sim 10^{-3}$ in agreement with the reported values in Williams et al. (4) and Rouzina and Bloomfield (6).

Because the model based on subsystems of cooperative length l accurately describes the quasi-static overstretching experiments, in Kinetics of the Chain: Sharp Interface, we extend our methods to study the kinetics of a system with sharp interfaces, meaning the phase transition takes place in a spatially homogeneous way.

TABLE 2 Calculation of the Zimm-Bragg cooperativity σ_F as a function of l using Eq. 25

l [bp]	Refers to	$\sigma_F \times 10^{-3}$	δF [pN]	δz [nm]
55	Fig. 3d	0.3	1.8	0.16
31	Fig. 3c	1.0	2.8	0.19
25	Fig. 2a	1.6	3.1	0.20
22	Fig. 3a	2.0	3.4	0.21
15	Fig. 4b	4.3	4.5	0.23

As a reference value, Williams et al. (4) and Rouzina and Bloomfield (6) measured $\sigma \approx 10^{-3}$ in DNA overstretching experiments at room temperature and $I = 150$ mM.

Kinetics of the chain: sharp interface

Next, we consider the kinetics of a single chain unit of length l. As before in Methods: Statistical Mechanics of the Chain, we assume that u corresponding to a single chain unit is independent of s, which leads to a spatially homogeneous transition along each unit. The order parameter u is now the relevant macroscopic variable describing the dynamic process over time t. Due to the effects of thermal fluctuations in the fast changing microscopic variables, the evolution of $u(t)$ is stochastic in nature and it obeys the Langevin equation (35). Bongini et al. (32) found that the kinetic mechanism during the transition involves viscosity-dependent delocalized motions at low frequency. Hence, we consider the case of spatial-diffusion-limited rate theory (35), where the kinetic equation of the overdamped system can be simplified to

$$\partial_t u(t) = \gamma\left[-\partial_u H_j(u)\right] + \sqrt{2\gamma k_B T}\,\overline{\xi}(t), \tag{27}$$

where H_j is the potential of a subsystem of length l given by Eq. 7, γ is the kinetic coefficient, and the Gaussian noise term $\overline{\xi}(t)$ is defined in terms of the Dirac delta function $\delta(x)$:

$$\left\langle \overline{\xi}(t_1)\overline{\xi}(t_2)\right\rangle = \delta(t_1 - t_2). \tag{28}$$

Equation 27 describes the classical problem of the diffusion of a particle (unit) $j \in n$, with probability density function $\rho(u,t)$, which is moving in a potential field H_j. The inset of Fig. 6 shows the potential for $C = 0$, which is characterized by the two stable minima $\pm u_o$ and an energy barrier E_l with maximum value at the unstable solution $u_b = 0$. For the overdamped case, the time evolution of $\rho(u,t)$ is governed by the Smoluchowski equation (35) and following Kramer's methodology for $E_l >> k_B T$ (47), we can determine the steady-state escape rates. The details of the procedure to obtain the rate from B-to-overstretched (k_L) and overstretched-to-B (k_R) using the potential $H_j(u)$ are shown in

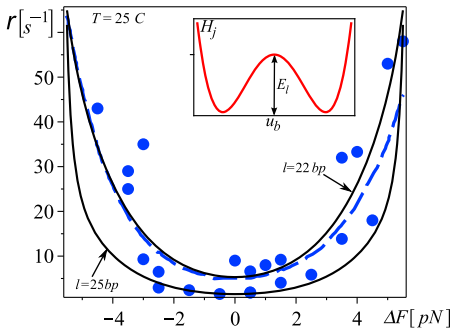

FIGURE 6 Relaxation rate $r = k_L + k_R$ in dsDNA overstretching experiments at $I = 150$ mM. (*Blue markers*) 2-pN force-step experiments in Bongini et al. (32), where $F_c \approx 66$ pN. (*Blue dashed line*) Fit used in Bongini et al. (32), where the authors combined their experimental measurements with Kramer-Bell theory. (*Black solid lines*) Theoretical predictions from expressions in Bosaeus et al. (29) using $l = 22$ and 25 bp. Here we have used $\gamma \sim 200$. To see this figure in color, go online.

Section S3, Chain Kinetics in the Supporting Material. The final results are

$$\begin{aligned} k_L &= \sqrt{\frac{k_B T}{2\pi}}\left(\frac{w_b \gamma}{Z_1 + Z_2}\right), \\ k_R &= \sqrt{\frac{k_B T}{2\pi}}\left(\frac{w_b \gamma}{Z_1 - Z_2}\right), \end{aligned} \tag{29}$$

where w_b is the curvature that results from linearizing the potential $H_j(u)$ about the unstable solution u_b (35) and

$$Z_1 = \sum_{m=0}^{\infty} \frac{(\beta C l)^{2m}}{(2m)!}\,\frac{\Phi(m)}{2}, \tag{30}$$

$$Z_2 = \sum_{\widehat{m}=0}^{\infty} \frac{(\beta C l)^{2\widehat{m}+1}}{(2\widehat{m}+1)!}\,\frac{\Phi\left(\widehat{m}+\frac{1}{2}\right)}{2}, \tag{31}$$

$$\Phi(x) = \frac{\Gamma(x + 1/2)}{(2\beta A_4 l)^{(2x+1)/4}} \exp\left(\frac{q^2}{4}\right) U(x,q). \tag{32}$$

The parameter $q^2 = 2\beta E_l$ is given by Eq. 14. Therefore, the rates can be cast in the familiar Arrhenius type form of

$$k_i = \Upsilon(F,T)\exp(-\beta E_l), \tag{33}$$

where $i = [L, K]$, $E_l >> k_B T$ is the energy barrier evaluated at $C = 0$ (see Eq. S3 in the Supporting Material), and Υ is a function of the external parameters F and T.

Next, we let n_B be the number of j segments in B-state and n_S be the number of segments in the overstretched state. Then, at any instant in time, the total number of segments $n = n_B + n_S$ is conserved. Therefore, the change of n_B as a function of time is given by

$$\frac{dn_B}{dt} = -k_L n_B + k_R n_S = -r n_B + k_R n, \tag{34}$$

where $r = k_L + k_R$ is the relaxation rate (35). The solution of the first-order ordinary differential equation (Eq. 34) is

$$\frac{n_B}{n} = \left(\frac{k_R + \alpha \exp[-rt]}{r}\right), \tag{35}$$

$$\frac{n_s}{n} = \left(\frac{k_L - \alpha \exp[-rt]}{r}\right), \tag{36}$$

where α is the integration constant and the equilibrium steady-state values are

$$\begin{aligned} \frac{\widehat{n}_B}{n} &= \frac{k_R}{r}, \\ \frac{\widehat{n}_S}{n} &= \frac{k_L}{r}. \end{aligned} \tag{37}$$

Finally, the equilibrium probability of segments in the overstretched state can be expressed as

$$P_s = \frac{\widehat{n}_S}{n} = \frac{1}{2} - \frac{Z_2}{2Z_1}, \tag{38}$$

where Z_2 and Z_1 are given by Eqs. 30 and 31.

In Fig. 6, we compare the experimental measurements of Bongini et al. (32) for the relaxation rate r with the predictions of our model. Using the same values of A_2, A_4, and l that resulted from the force-extension curve analysis at the same experimental conditions (see Fig. S1 *a*), we are able to accurately reproduce their experimental findings. The only fitting parameter is the kinetic coefficient, which we find to be $\gamma = 200$. Using $l = 22$ bp and assuming γ constant, our predictions for the relaxation rate $r_{\min}$ (corresponds to $F = F_c$) as a function of T, yielding a range of values $r_{\min} = 55\ \mathrm{s}^{-1}$ at $T = 25°\mathrm{C}$ to $r_{\min} = 3.2\ \mathrm{s}^{-1}$ at $T = 10°\mathrm{C}$. These are in agreement with the values reported in Bongini et al. (32), where $r_{\min} \in [3.5, 7.1]\ \mathrm{s}^{-1}$ is approximately constant for the same range of temperatures. Using the same parameters as in Fig. 6, in Fig. S4 we show a fit to another set of data in Bongini et al. (32), where the authors have used a different loading protocol.

One of the protocols used by Bongini et al. (32), denominated by the authors "square-wave protocol", consisted of instantaneously applying and reversing a large force step S_F. During the loading phase, F is instantaneously changed from $F^{(1)} << F_C$ (entire molecule is in the B form), up to a value of $F^{(2)} \approx F_c$ (midpoint of the transition). After the system reaches equilibrium, at time t_2 it is unloaded using an instantaneous change in force of the same magnitude from F_c to $F^{(3)}$ (32). In conditions at which the M form is energetically unfavorable in comparison to the S form ($T = 10°\mathrm{C}$ and $I = 150$ mM) (26,28), Bongini et al. (32) studied the transient kinetics using the square-wave protocol going from $F^{(3)} = F^{(1)} = 47$ pN to $F^{(2)}$ slightly larger than F_c. Their findings for the lengthening and shortening responses in the absence of melting coincide with the behavior described by our theoretical predictions. In Fig. 7, we present the theoretical solution for a dsDNA molecule undergoing a B-to-S transition. We use $l = 22$ bp and $\overline{L} = 1.7\ L$, values corresponding to an overstretching transition close to a pure S-form (see Experimental Observables: DNA Extension Z).

To model the large force-step lengthening experiment, we set the initial condition at time t_1 to be $n_s(t_1) = 0$ (dsDNA in B-form initially), which yields $\alpha = k_L$ in Eq. 26. The red line in Fig. 7 shows the theoretical calculation of the evolution of the fraction of segments n_s/n in the loading phase for $F^{(1)} << F_c$. For $F^{(2)} = F_c$, the system reaches steady state in ~1 s in agreement with the experiments of Bongini et al. (32) and the timescale measurements of the B-to-S transition reported in Rouzina et al. (30). During the unloading phase (shortening), the initial condition is $n_s(t^2) = n/2$,

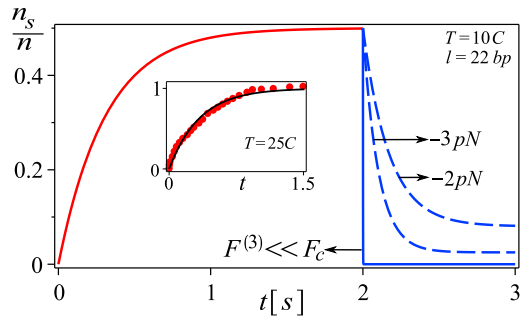

FIGURE 7 Transient kinetics: B-to-S and S-to-B. Force-jumps during loading and unloading a dsDNA molecule at $T = 10°\mathrm{C}$. As before, we use $\gamma = 200$, $l = 22$ bp, and $\overline{L} = 1.67\ L$. (*Red solid line*) Exponential evolution of n_s/n in time during loading phase. At $t_1 = 0$, F is instantaneously changed from $F^{(1)}$ to $F^2 = F_c$. The system reaches steady state in ~1 s. (*Blue lines*) Evolution during the unloading phase. At $t_2 = 2$ s, F is instantaneously dropped applying a force step $S_F = F^{(3)} - F_c$. For $S_F = -2$ and -3 pN (*blue dashed lines*), there is exponential decay behavior, whereas for $F^{(3)} << F_c$ (*blue solid*), $n_s \to 0$ rapidly. (*Inset*) Lengthening ($\Delta L/\Delta L_e$) as a function of time for a partially melted molecule (S and M). (*Red markers*) Data from Bongini et al. (32); (*black line*) our prediction using the same parameters as in Fig. 6 ($l \approx 15$ bp). To see this figure in color, go online.

such that $\alpha = (k_L - k_r)/2$ in Eq. 36. After the force is suddenly dropped to $F^{(3)} = F^{(1)}$ there is no exponential time course during the unloading, rather an abrupt instantaneous change in the extension of the molecule (32). The blue solid line in Fig. 7 shows that our predictions for n_s/n during unloading and $F^{(3)} = F^{(1)}$ match the experimental evidence, by depicting a sudden (almost instantaneous) change from $n_2 = 0.5$ to 0. This behavior can easily be understood in the context of our theory in the following way: For any applied force step ($S_F = F^{(3)} - F_c$) < 0, the left well in H_j will become deeper than the right well, and the population of segments in the right well will diffuse into the left well ($k_R > k_L$). For sufficiently small $F^{(3)} << F_c$, the expression n_s/n in Eq. 36 can be approximated to be

$$\frac{n_s}{n} \approx \frac{\exp(-k_R t)}{2} \text{ as } \frac{k_L}{k_R} \to 0, \tag{39}$$

and for $t > 0$, the fraction $n_s/n \to 0$ rapidly. The dashed blue lines in Fig. 7 show the time evolution of n_s/n during the unloading phase for different force steps ($S_F = F^{(3)} - F_c$).

Bongini et al. (32) also conducted the same square-wave protocol experiment at $T = 25°\mathrm{C}$, where it is possible the S and M forms start to mix in the overstretched state, so the authors denominated this experiment the kinetics in a partially melted molecule. The shortening transient was characterized by two different processes:

1. Stepwise shortening corresponding to the S-to-B transition (32); and
2. A much slower (~10 s) process, likely to correspond to a rate-limiting reannealing of the melted segments (32).

On the other hand, during the lengthening transient of the partially melted DNA at $T = 25°C$, the overall exponential behavior characteristic of the B-to-S transition remains (32).

As mentioned earlier, the hysteretic behavior during the overstretching transitions is mainly seen during unloading, while in the pulling phase the system is likely to be closer to equilibrium at all times. The difference in time that it takes the molecule to melt in comparison to the time taken by the molecule's recombination during unloading can explain the asymmetric hysteresis (14). We already know that the kinetic two-state model presented in this study accurately captures the time course of the nonhysteretic B-to-S transition at $T = 10°C$, therefore, in the analysis of the lengthening transient at $T = 25°C$ in Bongini et al., a two-state model with a lumped overstretched state where the S form is predominant is somehow justified. The inset of Fig. 7 shows the length change from B-to-overstretched ($\Delta L/\Delta L_e \approx n_s/\hat{n}_s$) as a function of time, where ΔL_e is the length measurement at steady state. Solid line corresponds to the theoretical solution at $T = 25°C$ and $F^{(2)} = F_c$ with the same parameters as in Fig. 6 ($l \approx 25$ bp), and red markers correspond to data from Fig. 1C in Bongini et al. (32). Although for $F_c = F^{(2)}$ the system reaches steady state in ~1.5 s, for $|F_c = F^{(2)}| > 0$, our model predicts the system will reach steady state faster. This last feature is also present in Bianco et al. (31) and Bongini et al. (32).

As a final remark, we point out that assuming $\gamma \approx 200$ remains independent of ionic concentration, the relaxation rate ($r_{\min}$) values for the four fits in Fig. 3 are of similar magnitude. Therefore, our methods predict that during a force-step pulling experiment, the time it takes the system to reach steady state at F_c ($t \approx 5{r_{\min}}^{-1}$), is ~< 1 for all four experimental conditions in Fig. 3. Given that Zhang et al. (26) uses a pulling protocol of 1 pN/s, this means, according to our loading curve fits, that the molecule has enough time to reach equilibrium. We also calculated the effect of l on τ (see Fig. S7), which shows that τ increases very quickly with l. In fact, when using the parameters from Fig. 3 *d*, if l was to increase from 60 to 80 bp, τ would increase by factor of 10, and at a 1 pN/s pulling rate, hysteresis would be seen.

We conclude that for conditions when the M-form starts to become energetically more favorable, i.e., extremely low salt concentrations and/or very high temperatures $T >$ 30°C, it is possible that $l \rightarrow 100$ bp in dsDNA overstretching experiments. However, at the same time, we are likely to see hysteresis effects during both loading and unloading. We think this could be the case in the experimental curves in Zhang et al. (26) at $I = 3.5$ mM and $T > 34°C$, where there is some hysteretic behavior even during the pulling phase. The presence of hysteresis during lengthening and shortening precludes the use of our methods to extract the l value from the overstretching curves. However, hysteretic effects can be greatly reduced by increasing the waiting times during pulling. In fact, times of ≈1 min have been reported to be sufficient to completely reach equilibrium (42).

The results presented in this section provide insights into the kinetics of the system as a function of the imposed force F. However, the study of the kinetics of a phase transition cannot be complete without an analysis of the nucleation and propagation of interfaces. In Section S5, Kinetics of the Chain with Finite Size Interfaces: Domain Walls in the Supporting Material, we present a summary of the kinetic analysis including domain walls near the transition point $F_c = F$. The results of Section S5, Kinetics of the Chain with Finite Size Interfaces: Domain Walls in the Supporting Material on the kinetic analysis including propagating interfaces further validates the approximation of sharp interface presented in this section. Both solution methods share the same qualitative characteristics.

CONCLUSIONS

In this article, we have explained two features in torsionally unconstrained DNA undergoing an overstretching transition—force-extension relations and kinetics. First, we introduced a model for the statistical mechanics of a chain composed of n segments of length l (the measure of cooperativity of the system), in which we neglect the spatial fluctuations of $u(s)$ within each segment of the chain. We assume that each segment is perfectly homogeneous at any instant in time and we focus on studying the global statistical fluctuations of u. By doing so we are able to obtain an analytical expression for the end-to-end extension $\langle z \rangle$ of the filament as a function of force F, temperature T, and the segment's length l. In agreement with the conclusion from the experiments of Bongini et al. (32), we found by fitting several sets of data from numerous groups (25,26,28,31,32) that independently of length L, temperature T, or ionic concentration I, if the extension of the overstretched state is ~1.7 L, the cooperative length is $l \approx 25$ bp.

In this situation, S-DNA is the preferred overstretched state. As the extension of the overstretched state decreases to ~1.5 L, for conditions at which the M-form can compete with the S-form, we found $l > 30$ bp is required to fit the lengthening curves in Zhang et al. (26). There is, in fact, experimental evidence supporting the idea that for a range of temperatures and low-to-moderate salt concentration there would be a mixed overstretched state (S and M) (26,28,32). The larger values $l > 50$ bp approach the measurements corresponding to the B-to-M transition ($l \sim$ 100 bp) reported by Rouzina et al. (30). This feature would further support the idea that the ~1.5 L overstretched DNA is in fact M + S. Therefore, our model can be practical in using extension $\langle z \rangle$ and l as parameters to quantify the fractions in the mixed overstretched state, where values of l close to 25 bp would indicate an overstretched DNA form closer to the S-DNA, whereas larger values of l would

indicate an increase in the M-DNA content in the overstretched form.

In Kinetics of the Chain: Sharp Interface, we extended our theory to encompass the kinetics of the chain under the assumption of an overdamped system based on experimental evidence (32). Our kinetic results further support our two-state cooperative model. We show that the theoretical predictions for the relaxation rates r and the system's exponential time course are consistent with the results seen in experiments and simulations (31,32). Our calculations show that the time required to reach steady state in a transition to an overstretched state where the S-form is predominant is $\tau \sim 1$ s, which agrees with the timescale reported in the B-to-S transition (30).

An important aspect of our theory is that the probability of segments in the overstretched state P_s and the width of the transition δF depend on the cooperativity unit l, temperature T, and the parameters A_2 and A_4. However, as long as the ratio A_2/A_4 remains the same, the specific values of these parameters do not affect P_s and δF significantly. Therefore, our model can provide significant insight in the overstretching transition with knowledge of the relative extension of the overstretched phase

$$\left(\overline{L}/L - 1\right) \sim \sqrt{2A_2/A_4},$$

which is an easy variable to determine in experiments. (In Fig. S5, we present solutions of P_s and $\langle u \rangle$ for different values of A_4, while keeping the ratio A_2/A_4 constant.)

During DNA overstretching, Bianco et al. (31) and Bongini et al. (32) found the transition state is almost midway between compact and extended states. This supports the use of a symmetric potential as done in this study. Our analytical model proves to be a useful tool by capturing some key features of the transition, although there are still several interactions that could influence the transition which our model cannot accommodate. For example, there is evidence that the percentage of GC versus AT tracts plays an important role in the transition (29), and for this level of detail, basepair or rigid-base models are required (48,49). The slower relaxation rates of a partially melted molecule that result in different hysteretic behavior during the loading and unloading phase in overstretching experiments cannot be captured by our symmetric model, and a dynamic mesoscopic Peyrard-Bishop-Dauxois potential has been proposed to account for this asymmetric behavior (14).

Similarly, the coarse-grained simulations of Whitelam et al. (15–17) have successfully integrated some of the dsDNA microscopic detail required to account for DNA sequence effects and the asymmetric hysteretic behavior during the overstretching transition. Finally, we do not expect our model to capture the transition to single-stranded DNA (peeled DNA), because thermal fluctuation will play a larger role in the extensibility of the peeled structure even at high forces, leading to markedly asymmetric force extension curves (softer after the transition). However, our methods can be combined with asymmetric potentials, such as piecewise quartic energies with a cubic term (see Section S4, Asymmetric Potentials in the Supporting Material), which could help to account for asymmetric behavior present in single-molecule stretching experiments.

In addition to applications to DNA phase changes, two-state models have been used to interpret experiments on partially unfolded protein oligomers (50) and to study the mechanical behavior of small molecule binding to DNA (51). The binding of proteins or small-molecules to dsDNA can produce coupled conformational changes that affect the binding of subsequent proteins (molecules), often over a long range in the dsDNA (52). Binding of the RecA protein to dsDNA lengthens the molecule by ~1.5 times and it has been shown that overstretching promotes RecA nucleation and polymerization along dsDNA (53). Similarly, an ~50% increase in extension of DNA is observed upon interaction with EtBr and Rad 51 (54,55). Therefore, it is possible, in protein-dsDNA complexes, for the conformational changes caused by small-molecule binding to be coupled with external mechanical forces. Our theoretical framework to study the dsDNA overstretching transition can be useful in describing certain aspects present during conformational changes in DNA-protein complexes.

SUPPORTING MATERIAL

Eight figures, and additional supplemental information are available at http://www.biophysj.org/biophysj/supplemental/S0006-3495(14)00953-9.

We acknowledge partial support through a National Science Foundation CAREER award (grant No. NSF CMMI-0953548) and through the Nano/Bio Interface Center at the University of Pennsylvania (grant No. NSF DMR08-32802).

REFERENCES

1. Marko, J. F., and S. Neukirch. 2013. Global force-torque phase diagram for the DNA double helix: structural transitions, triple points, and collapsed plectonemes. *Phys. Rev. E Stat. Nonlin. Soft Matter Phys.* 88:062722.
2. Bustamante, C., Z. Bryant, and S. B. Smith. 2003. Ten years of tension: single-molecule DNA mechanics. *Nature.* 421:423–427.
3. Smith, S. B., Y. Cui, and C. Bustamante. 1996. Overstretching B-DNA: the elastic response of individual double-stranded and single-stranded DNA molecules. *Science.* 271:795–799.
4. Williams, M. C., I. Rouzina, and V. A. Bloomfield. 2002. Thermodynamics of DNA interactions from single molecule stretching experiments. *Acc. Chem. Res.* 35:159–166.
5. Williams, M. C., J. R. Wenner, …, V. A. Bloomfield. 2001. Entropy and heat capacity of DNA melting from temperature dependence of single molecule stretching. *Biophys. J.* 80:1932–1939.
6. Rouzina, I., and V. A. Bloomfield. 2001. Force-induced melting of the DNA double helix 1. Thermodynamic analysis. *Biophys. J.* 80: 882–893.
7. Cluzel, P., A. Lebrun, …, F. Caron. 1996. DNA: an extensible molecule. *Science.* 271:792–794.

8. Ahsan, A., J. Rudnick, and R. Bruinsma. 1998. Elasticity theory of the B-DNA to S-DNA transition. *Biophys. J.* 74:132–137.
9. Marko, J. 1998. DNA under high tension: overstretching, underwinding, and relaxation dynamics. *Phys. Rev. E Stat. Phys. Plasmas Fluids Relat. Interdiscip. Topics.* 57:2134–2149.
10. Storm, C., and P. C. Nelson. 2003. Theory of high-force DNA stretching and overstretching. *Phys. Rev. E Stat. Nonlin. Soft Matter Phys.* 67:051906.
11. Storm, C., and P. Nelson. 2003. The bend stiffness of S-DNA. *Europhys. Lett.* 62:760–766.
12. Cizeau, P., and J. Viovy. 1997. DNA: an extensible molecule. *Biopolymers.* 42:383–385.
13. Fiasconaro, A., and F. Falo. 2012. Dynamical model for the full stretching curve of DNA. *Phys. Rev. E Stat. Nonlin. Soft Matter Phys.* 86: 032902.
14. Pupo, A. E., F. Falo, and A. Fiasconaro. 2013. DNA overstretching transition induced by melting in a dynamical mesoscopic model. *J. Chem. Phys.* 139:095101.
15. Whitelam, S., S. Pronk, and P. L. Geissler. 2008. Stretching chimeric DNA: a test for the putative S-form. *J. Chem. Phys.* 129:205101.
16. Whitelam, S., P. L. Geissler, and S. Pronk. 2010. Microscopic implications of S-DNA. *Phys. Rev. E Stat. Nonlin. Soft Matter Phys.* 82: 021907.
17. Whitelam, S., S. Pronk, and P. L. Geissler. 2008. There and (slowly) back again: entropy-driven hysteresis in a model of DNA overstretching. *Biophys. J.* 94:2452–2469.
18. Laughton, C. A., and S. A. Harris. 2011. Atomistic simulation of DNA. *Comput. Mol. Sci.* 1:6590–6600.
19. Lebrun, A., and R. Lavery. 1996. Modeling extreme stretching of DNA. *Nucleic Acids Res.* 24:2260–2267.
20. Kosikov, K. M., A. A. Gorin, …, W. K. Olson. 1999. DNA stretching and compression: large-scale simulations of double helical structures. *J. Mol. Biol.* 289:1301–1326.
21. Cheatham, 3rd, T. E., and P. A. Kollman. 2000. Molecular dynamics simulation of nucleic acids. *Annu. Rev. Phys. Chem.* 51:435–471.
22. Konrad, M., and J. Bolonick. 1996. Molecular dynamics simulation of DNA stretching is consistent with the tension observed for extension and strand separation and predicts a novel ladder structure. *J. Am. Chem. Soc.* 118:10989–10994.
23. Harris, S. A., Z. A. Sands, and C. A. Laughton. 2005. Molecular dynamics simulations of duplex stretching reveal the importance of entropy in determining the biomechanical properties of DNA. *Biophys. J.* 88:1684–1691.
24. Bongini, L., V. Lombardi, and P. Bianco. 2014. The transition mechanism of DNA overstretching: a microscopic view using molecular dynamics. *J. R. Soc. Interface.* 11:20140399.
25. Zhang, X., H. Chen, …, J. Yan. 2012. Two distinct overstretched DNA structures revealed by single-molecule thermodynamics measurements. *Proc. Natl. Acad. Sci. USA.* 109:8103–8108.
26. Zhang, X., H. Chen, …, J. Yan. 2013. Revealing the competition between peeled ssDNA, melting bubbles, and S-DNA during DNA overstretching by single-molecule calorimetry. *Proc. Natl. Acad. Sci. USA.* 110:3865–3870.
27. Fu, H., H. Chen, …, J. Yan. 2011. Transition dynamics and selection of the distinct S-DNA and strand unpeeling modes of double helix overstretching. *Nucleic Acids Res.* 39:3473–3481.
28. King, G. A., P. Gross, …, E. J. Peterman. 2013. Revealing the competition between peeled ssDNA, melting bubbles, and S-DNA during DNA overstretching using fluorescence microscopy. *Proc. Natl. Acad. Sci. USA.* 110:3859–3864.
29. Bosaeus, N., A. H. El-Sagheer, …, B. Nordén. 2012. Tension induces a base-paired overstretched DNA conformation. *Proc. Natl. Acad. Sci. USA.* 109:15179–15184.
30. Rouzina, I., M. McCauley, and M. Williams. 2013. Kinetics of DNA overstretching: melting versus B-To-S transition. *Biophys. J.* 104:165A.
31. Bianco, P., L. Bongini, …, V. Lombardi. 2011. PicoNewton-millisecond force steps reveal the transition kinetics and mechanism of the double-stranded DNA elongation. *Biophys. J.* 101:866–874.
32. Bongini, L., L. Melli, …, P. Bianco. 2014. Transient kinetics measured with force steps discriminate between double-stranded DNA elongation and melting and define the reaction energetics. *Nucleic Acids Res.* 42:3436–3449.
33. Chan, H. S., S. Bromberg, and K. A. Dill. 1995. Models of cooperativity in protein folding. *Philos. Trans. R. Soc. Lond. B Biol. Sci.* 348:61–70.
34. Jackson, M. 2006. Molecular and Cellular Biophysics. Cambridge University Press, New York.
35. Hanggi, P., P. Talkner, and M. Borkovec. 1990. Reaction-rate theory: fifty years after Kramers. *Rev. Mod. Phys.* 62:251–341.
36. Landau, L. D., and E. Lifshitz. 1980. Statistical Physics, 3rd Ed. Pergamon Press, New York, Pt. 1.
37. Tuszynski, J. A., M. J. Clouter, and H. Kiefte. 1986. Non-Gaussian models for critical fluctuations. *Phys. Rev. B Condens. Matter.* 33:3423–3435.
38. Odijk, T. 1995. Stiff chains and filaments under tension. *Macromolecules.* 28:7016–7018.
39. Roy, B. N. 2002. Fundamentals of Classical and Statistical Thermodynamics. Wiley, New York.
40. Ryzhik, I., and I. Gradshteyn. 1980. Tables of Integrals, Series, and Products. Academic Press, London.
41. Olver, F. W. J., D. W. Lozier, …, C. W. Clark (editors). 2010. NIST Handbook of Mathematical Functions. Cambridge University Press, New York.
42. Sarkar, A., J. F. Léger, …, J. F. Marko. 2001. Structural transitions in DNA driven by external force and torque. *Phys. Rev. E Stat. Nonlin. Soft Matter Phys.* 63:051903.
43. van Mameren, J., P. Gross, …, E. J. Peterman. 2009. Unraveling the structure of DNA during overstretching by using multicolor, single-molecule fluorescence imaging. *Proc. Natl. Acad. Sci. USA.* 106: 18231–18236.
44. Wenner, J., M. Williams, …, V. Bloomfield. 2002. Salt dependence of the elasticity and overstretching transition of single DNA molecules. *Biophys. J.* 82:3160–3169.
45. Nelson, P. 2008. Biological Physics: Energy, Information, Life. W.H. Freeman, New York.
46. Khokhlov, A. R., and A. Y. Grosberg. 1994. Statistical Physics of Macromolecules. American Institute of Physics, New York.
47. Kramer, H. 1940. Brownian motion in a field of force and the diffusion model of chemical reactions. *Physica.* 7:284–304.
48. Gonzalez, O., D. Petkevičiūtė, and J. H. Maddocks. 2013. A sequence-dependent rigid-base model of DNA. *J. Chem. Phys.* 138:055102.
49. Olson, W. K., and V. B. Zhurkin. 2000. Modeling DNA deformations. *Curr. Opin. Struct. Biol.* 10:286–297.
50. Su, T., and P. K. Purohit. 2010. Thermodynamics of a heterogeneous fluctuating chain. *J. Mech. Phys. Solids.* 58:164–186.
51. Argudo, D., and P. K. Purohit. 2013. Torsion of DNA modeled as a heterogeneous fluctuating rod. *J. Mech. Phys. Solids.* 62:228–256.
52. Schurr, J. M., J. J. Delrow, …, A. S. Benight. 1997. The question of long-range allosteric transitions in DNA. *Biopolymers.* 44:283–308.
53. Leger, J. F., J. Robert, …, J. F. Marko. 1998. RecA binding to a single double-stranded DNA molecule: a possible role of DNA conformational fluctuations. *Proc. Natl. Acad. Sci. USA.* 95:12295–12299.
54. Lipfert, J., S. Klijnhout, and N. H. Dekker. 2010. Torsional sensing of small-molecule binding using magnetic tweezers. *Nucleic Acids Res.* 38:7122–7132.
55. Lee, M., J. Lipfert, …, N. H. Dekker. 2013. Structural and torsional properties of the RAD51-dsDNA nucleoprotein filament. *Nucleic Acids Res.* 41:7023–7030.